ELSEVIER

Journal of Nuclear Materials 318 (2003) 228–233

journal of nuclear materials

www.elsevier.com/locate/jnucmat

Low temperature tensile properties of steels containing high concentrations of helium

H. Ullmaier *, J. Chen

ESS-Projekt im Forschungszentrum Jülich, D-52425 Jülich, Germany

Abstract

Due to the high particle energies, the radiation conditions in spallation targets are characterized by very high helium production rates. We simulated this fast helium generation by implantation of α-particles into AISI 316L and DIN 1.4914 specimens and studied its effect on the mechanical properties by subsequent tensile tests at 25 and 300 °C, respectively. Up to He-concentrations of 0.5 at.% the observed hardening and embrittlement can be attributed to displacement-induced defects. However, at around 1 at.% He, the observed increase in yield stress and decrease in ductility are considerably outside the trend lines for the dpa dependence. Such a 'critical' He-concentration was also inferred from hardness measurements on dual-beam irradiated specimens.The microstructure of the implanted specimens shows the usual features appearing in steels after low temperature irradiation ('black dot' damage and dislocation loops). No visible (>1 nm) bubbles could be detected in the specimens, including those containing 1 at.% He.

1. Introduction

The lifetime of vital structural components in nuclear devices is determined by radiation damage effects. They are caused by two basic interactions of the irradiation particles with the materials of the components: atomic displacements causing lattice defects and nuclear reactions producing foreign elements. Among the latter, helium is of particular concern since it is known to lead to drastic embrittlement already at very low concentrations.

It is customary to characterize the helium production in a material due to a given radiation environment by the so-called He to dpa ratio, i.e. the concentration of helium produced (in appm) per displacement per atom (dpa). Since the cross sections for He-production steeply increase with increasing particle energy, the He to dpa ratio is low in fission reactors, medium in fusion reactors and high in spallation sources (Fig. 1). More illustrative may be an absolute number: the He concentration generated in the center of the beam window in a 5 MW target of the planned European Spallation Source (ESS) after 1 year of full power operation would be close to 1 at.%.

Helium embrittlement as studied in fusion materials research is a typical high temperature effect and becomes virulent at temperatures above 0.4–0.5 of the melting temperature T_m [1], whereas the maximum operating temperature of the structural components in high power liquid mercury targets will never exceed 250 °C (<0.3 T_m for steels). Nevertheless, concerns about the low temperature mechanical behavior of materials are certainly justified for the aforementioned helium concentration, all the more as no experimental data for this parameter range exist.

At present data from specimens irradiated in a spallation environment up to doses of about 10 dpa/1500 appm He are available from spent targets (Los Alamos Neutron Science Center, Lansce, and ISIS) [2] and irradiation programs in Swiss Intensive Neutron Source (SINQ) [3] and LANSCE [4]. The above dose corresponds to a service time of about 2–5 months in ESS (5 MW) and SNS (2 MW), respectively. New experiments aiming for higher doses and including new types of specimens (e.g. for studying liquid metal embrittlement

* Corresponding author. Tel.: +49-24 6161 3160; fax: +49-24 6161 8675.

E-mail address: h.ullmaier@fz-juelich.de (H. Ullmaier).

0022-3115/03/$ - see front matter © 2003 Elsevier Science B.V. All rights reserved.
doi:10.1016/S0022-3115(03)00024-2

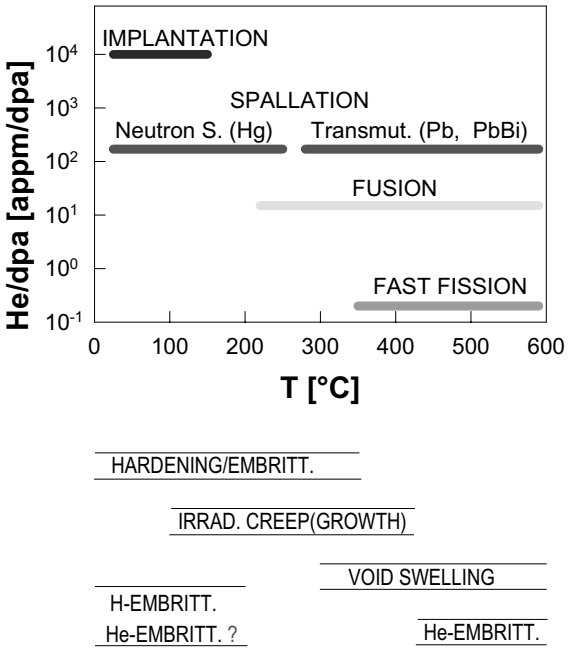

Fig. 1. Range of operating temperatures and helium to dpa ratios, respectively, for structural materials in different nuclear environments. In the lower part of the figure the temperature ranges of some critical radiation damage effects in steels are indicated.

under irradiation) have been started within the SINQ Test Irradiation Program (STIP) collaboration [5].

As a completion to these efforts, simulation irradiations in accelerators and reactors are carried out. In this contribution we report results on specimens implanted with α-particles at a cyclotron. This simulation method enables the homogeneous introduction of helium at accelerated rates (≈50 appm/h as compared to <0.2 appm/h in SINQ) into specimens suitable for tensile testing. Although the implantation also produces displacement damage, its space-averaged rate is rather low, leading to He to dpa rations of about 10^4 appm/dpa, i.e. about 60 times higher than under spallation conditions (Fig. 1). A direct transfer of such simulation data to the spallation case is therefore questionable. On the other hand, the results should be useful to uncover the basic mechanisms of the effect of helium on materials properties at temperatures below 0.3 T_m.

2. Experimental

Miniature tensile specimens have been prepared from two materials: Solution annealed (s.a.) austenitic stainless steel AISI 316L as the favored candidate material for the structural component of the SNS mercury target and martensitic steel DIN 1.4914 (MANET in the fusion program) under consideration for the ESS target container. After rolling the materials to a thickness of 0.1 mm (the range of the 28 MeV α-particles used), dogbone shaped tensile specimens were prepared by spark erosion. The gauge length and width were 10 and 3 mm, respectively.

After their final heat treatments in high vacuum, the specimens were soldered with indium to water cooled copper blocks each holding two specimens. Such a specimen holder was inserted into an irradiation chamber at a beam line of the Juelich CV 28 cyclotron.

The 28 MeV α-beam delivered by the cyclotron was wobbled in both lateral directions to achieve a homogeneous current density over the area of the aperture of 8×15 mm^2. The wobbling frequency of 10 kHz is high enough to disallow diffusion of surviving defects to sinks during a wobbling period. The height of the aperture is larger than the gauge length of the specimens, i.e. the implantation was extended into the wider shoulders of the specimens, ensuring that they failed in the gauge section in spite of their irradiation induced hardening. After the α-beam passed a thin Al window separating the accelerator vacuum from the vacuum in the irradiation chamber, the energy was varied before entering the specimen. This was achieved by Al degrader foils of different thickness mounted on the circumference of a wheel rotating in front of the specimen surface. Typical current densities of the α-beam were around 3.6 μA/cm^2, leading to helium introduction rates of about 50 appm/h homogeneously distributed over the implanted specimen volumes. The implantation temperature was always 25 °C.

After implantation the specimens were detached from the holders by heating them to a temperature slightly above the melting point of indium (156 °C). The tensile tests were performed in test machines designed to yield optimum results for miniaturized specimens. The test rig was inserted into a quartz tube which was surrounded by a furnace, thus allowing tests in vacuum in a temperature range from 25 to 500 °C. In this work, results at 25 and 300 °C, respectively, and strain rates of about 10^{-4} s^{-1} are reported. After tensile testing, the fracture surfaces of the samples were observed by SEM and Vickers hardness was measured using loads between 1 and 5 N.

Finally, TEM specimens were prepared from implanted volumes in the gauge sections (= strained) and the shoulders (= unstrained), respectively.

3. Results

3.1. 316L austenitic steel

Fig. 2 shows stress–strain curves obtained from tensile testing the 316L specimens at 25 and 300 °C, respectively. Without irradiation, the solution annealed

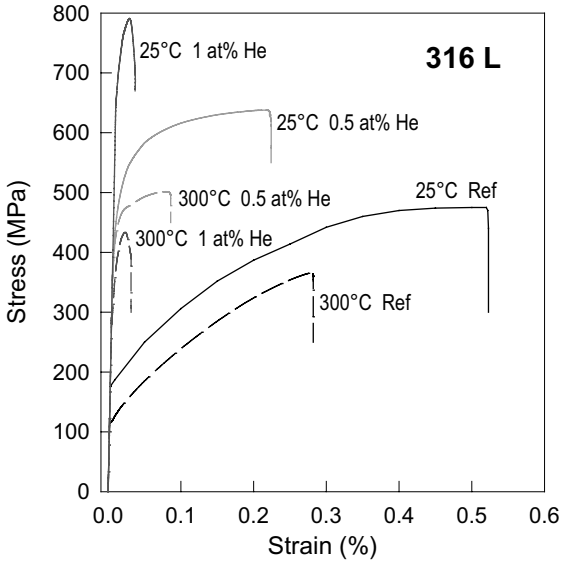

Fig. 2. Stress–strain curves in tensile tests at room temperature (RT, solid lines) and at 300 °C (dotted lines) of solution annealed 316 L specimens implanted with 0, 0.5 and 1 at.% helium at RT.

material is very soft and ductile but hardens rapidly with irradiation, together with a reduction of the strain to failure. The fracture mode, however, remains ductile (Fig. 3 (left)) up to helium concentrations of at least 0.5 at.% (≈0.5 dpa), whereas the 1 at.% specimens failed at both temperatures in a transgranular brittle manner (Fig. 3 (right)) without noticeable reduction in area.

TEM observation of the microstructure revealed that a high density of small defect clusters appearing as 'black dots' with an average size of 2 nm was formed during helium implantation to doses up to 0.5 at.%. For the specimens with 1 at.% helium (1 dpa), besides the 'black dots', sessile Frank loops with a mean size of 12 nm and density of 4.8×10^{22} m^{-3} were observed in addition to the dots. Helium bubbles could not be detected even in the specimens with 1 at.% helium. Fig. 4 shows an example of the microstructure of a sample with 1 at.% He. A typical post-deformation microstructural feature in specimens implanted with He concentrations up to 0.5 at.% is a high density of twin lamellae with {1 1 1} mirror planes. Their widths vary from a single atom layer (stacking fault) to several tens of nm. An example is given in Fig. 5 showing the microstructure in a specimen with 0.5 at.% He tested at 25 °C. Very similar microstructural features have been found in deformed 304L specimens irradiated in the LANSCE target [6]. Increasing the test temperature to 300 °C does not cause noticeable changes in the microstructure. It should be noted that twin lamellae could not be found in the deformed specimens containing 1 at.% He.

3.2. 1.4914 Martensitic steel

Fig. 6 shows stress–strain curves obtained from tensile testing the 1.4914 ('MANET') specimens at 25 and 300 °C, respectively. Although this material is much

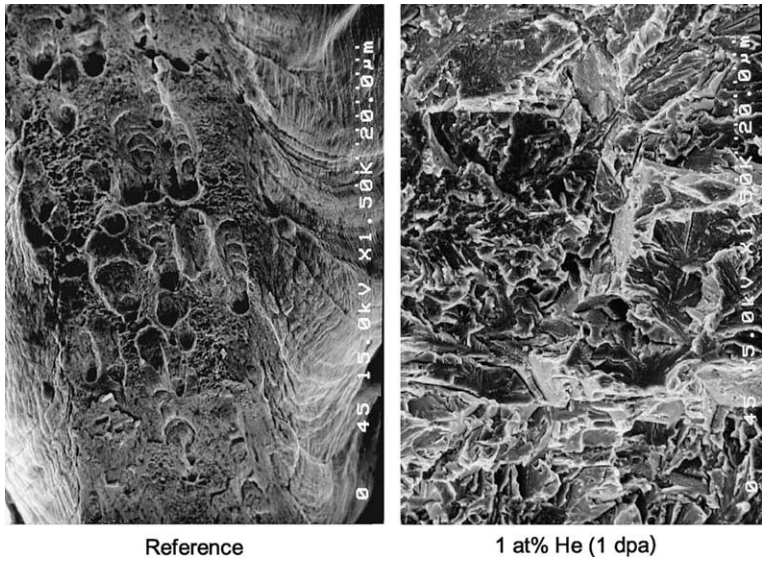

Fig. 3. SEM micrographs of the fracture surfaces of 316L specimens after tensile testing at RT containing 0 (left) and 1 at.% helium (right).

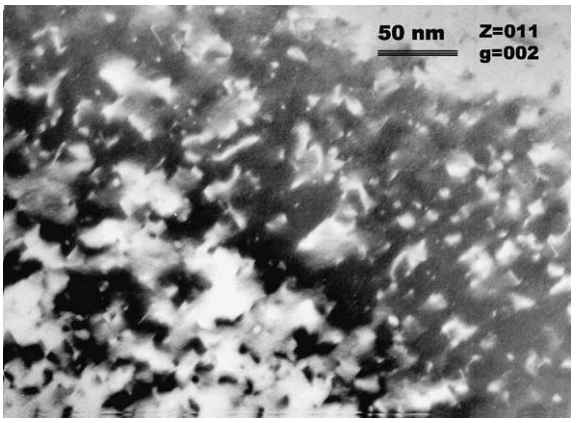

Fig. 4. Bright field TEM micrograph of 316L specimen with 1 at.% He showing black dots and faulted loops on {1 1 1} planes.

stronger than the s.a. austenitic steel in its initial state, appreciable hardening by irradiation is observed also in this case. Already in the unirradiated material the strains to necking are an order of magnitude smaller than in the austenitic steel and are further reduced by He-implantation. However, up to 0.5 at.% (≈0.5 dpa) the martensitic specimens also fail in a transgranular ductile manner. This is changed in the 1 at.% specimen which failed in the elastic range (Fig. 6) without any detectable plastic deformation (see also the right SEM micrograph of Fig. 7).

The microstructure of a sample with 1 at.% helium is illustrated in Fig. 8. A high density of 'black dots' is the main feature of the microstructure in the implanted and deformed sample. The average size of the small clusters

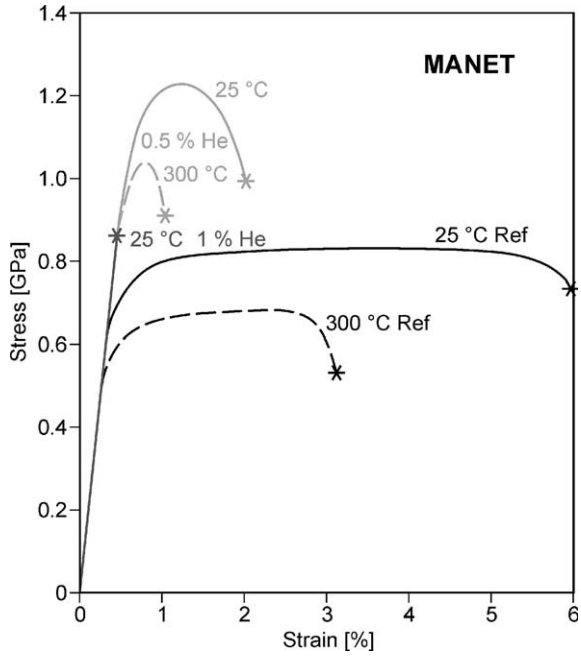

Fig. 6. Stress–strain curves in tensile tests at RT (solid lines) and at 300 °C (dotted lines) of 1.4914 martensitic steel specimens implanted with 0, 0.5 and 1 at.% helium at RT.

is 3.5 nm. As in 316L, no bubbles could be detected. Increasing the test temperature to 300 °C does not noticeably change the microstructure. A similar microstructure has been observed in 1.4926 martensitic steel irradiated in the LANSCE target [9].

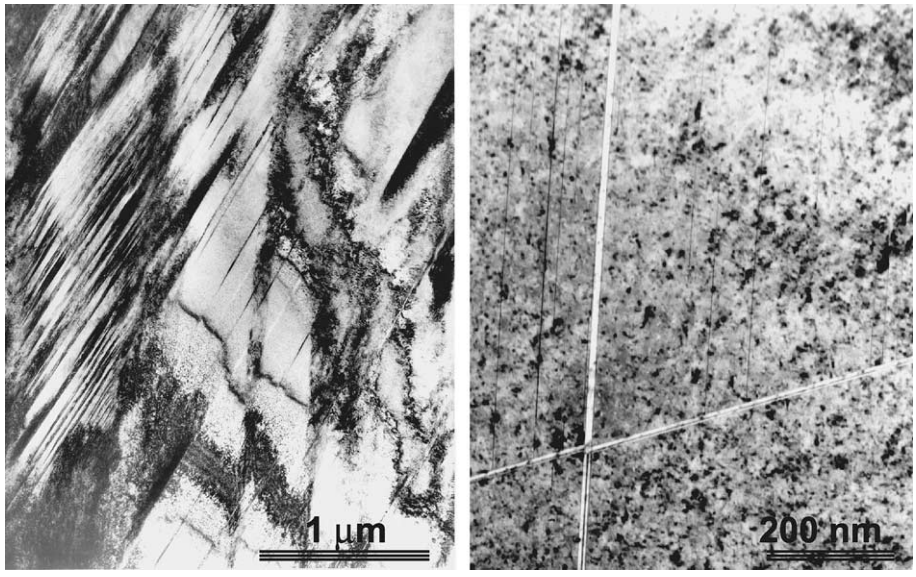

Fig. 5. Micrographs showing the twin structure in deformed 316L steel containing 0.5 at.% He.

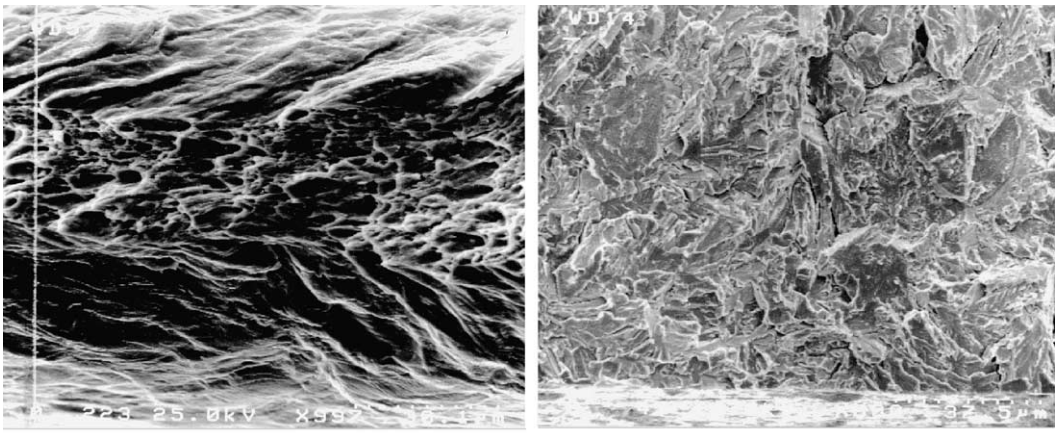

Fig. 7. SEM micrographs of the fracture surfaces of 1.4914 specimens after tensile testing at RT containing 0 (left) and 1 at.% helium (right).

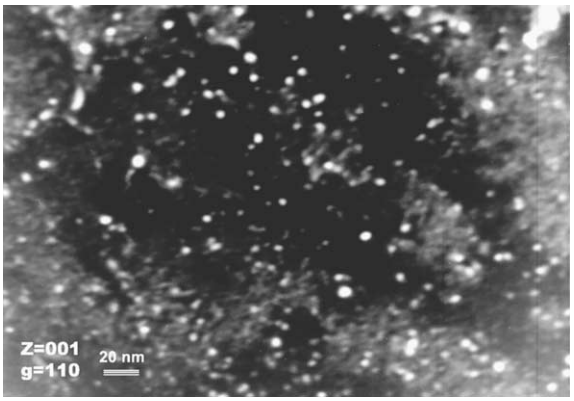

Fig. 8. Weak beam dark field TEM image of black dot damage in 1.4914 specimen containing 1 at.% He.

4. Discussion

In Fig. 9 the increase in yield stress $\Delta\sigma_{0.2}$ and the strain to necking ε_{STN} as taken from the stress–strain curves are given as a function of the displacement dose, together with values obtained by proton [7] and neutron [8] irradiations. The data follow trend lines independent of the irradiation particles (H, He, n), suggesting that the hardening is dominated by displacement defects as long as the helium concentration does not exceed 0.5 at.%. However, for He contents of around 1 at.% an additional hardening/embrittlement is observed which is distinctly outside the trend of the dpa-dependence. This behaviour is also reflected in the microstructure; although the 1 at.% specimens show a small plastic deformation before failure, the twin lamellae otherwise observed in deformed specimens (Fig. 5) are absent in this case.

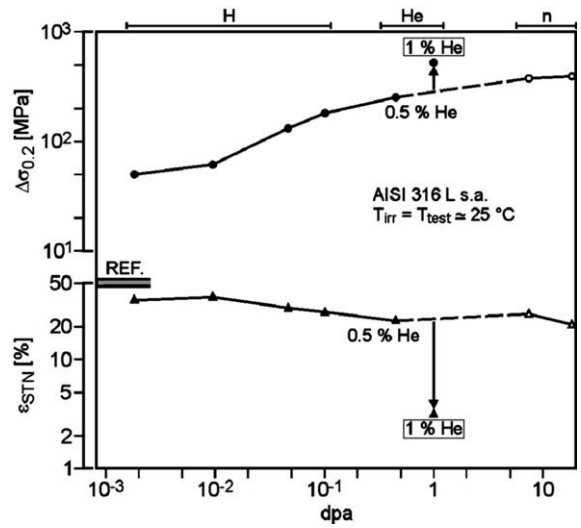

Fig. 9. Increase of yield stress, $\Delta\sigma_{0.2}$, and decrease of strain to necking, ε_{STN}, respectively, as function of the displacement dose for 316L.

A similar 'critical' concentration where helium seems to cause strong additional hardening is found in the martensitic steel. Fig. 10 gives the dependencies of the yield stress $\sigma_{0.2}$, the ultimate tensile strength σ_{UTS} and the strain to necking ε_{STN} at 25 °C as a function of the implanted He concentration and displacement dose, respectively. The failure stress of the 1 at.% specimen (filled square) is rather meaningless because its value is determined by surface flaws in the completely brittle material which failed in the elastic range (see Fig. 6). The helium effect in this material is thus even more drastic than in the relatively weak solution annealed austenitic

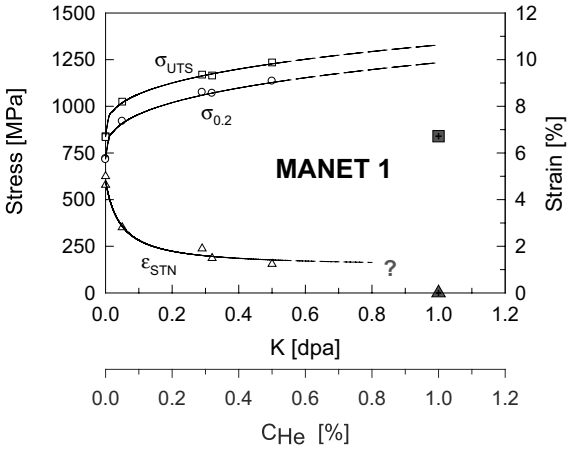

Fig. 10. Increase of yield stress and ultimate tensile strength and decrease of strain to necking, respectively, as a function of the displacement dose for 1.4914.

steel which retains at least a small remnant of its initial large ductility.

A 'critical' helium concentration of about 1 at.% suggested by the described results is supported by hardness measurements on 316LN steel implanted with low energy Fe and He ions, respectively [10].

Considering the properties of helium in metals and the microstructural observations, it is obvious that the usual (= high temperature) mechanism of helium embrittlement, weakening of the grain boundaries by bubbles, cannot account for the effects described here. Therefore a model has been developed which should be valid for the present parameter range: low temperatures ($< 0.3T_m$) and high He/dpa ratios. Its main features and a comparison of its predictions with the experimental results are given in Ref. [11].

Here we conclude with a remark on the practical aspect of the present results. Even under the most demanding conditions (center of 5 MW ESS target window), 1 at.% helium will be generated in times (>1 year of full power operation) which are safely above the target exchange periods. This means that helium should not be a lifetime-limiting factor for structural components in Hg-targets operating in a temperature range from RT 300 °C. This statement must be considered with caution because it is based on simulation results with a He/dpa ratio of 10^4 appm/dpa which is more than 50 times higher than in the spallation case. Theoretical considerations suggest that implantation presents the worst case only if referred to displacement dose but leads to a higher 'critical' helium concentration than in the spallation case (see Table 1 in Ref. [11]).

References

[1] H. Ullmaier, H. Trinkaus, Mater. Sci. Forum 97–99 (1992) 451.
[2] J. Chen et al., these Proceedings. doi:10.1016/S0022-3115(03)00007-2.
[3] Y. Dai, G.S. Bauer, J. Nucl. Mater. 296 (2001) 43.
[4] S.A. Maloy, M.R. James, G. Willcutt, W.F. Sommer, M. Sokolov, L.L. Snead, M.L. Hamilton, F. Garner, J. Nucl. Mater. 296 (2001) 119.
[5] Y. Dai, X.J. Jia, M. Häfeli, K. Geissmann, PSI Scientific and Technical Report 2001, vol. IV, p. 69, ISSN 1423 7350, March 2002.
[6] Y. Dai, X. Jia, J.C. Chen, W.F. Sommer, M. Victoria, G.S. Bauer, J. Nucl. Mater. 296 (2001) 174.
[7] H. Schroeder, W. Liu, J. Nucl. Mater. 191–194 (1992) 776.
[8] J.D. Elen, P. Fenici, J. Nucl. Mater. 191–194 (1992) 766.
[9] Y. Dai, G. Bauer, F. Carsughi, H. Ullmaier, S.A. Maloy, W.F. Sommer, J. Nucl. Mater. 265 (1999) 203.
[10] J.D. Hunn, E.H. Lee, T.S. Byun, L.K. Mansur, J. Nucl. Mater. 282 (2000) 131.
[11] H. Trinkaus, these Proceedings. doi:10.1016/S0022-3115(03)00103-X.